SANDIA REPORT

SAND2004-1059
Unlimited Release
Printed March, 2004

Molecular Simulations of MEMS and Membrane Coatings (PECASE)

Turkan Aydogmus, Asad Javaid, David M. Ford and Aidan P. Thompson

Prepared by
Sandia National Laboratories
Albuquerque, New Mexico 87185 and Livermore, California 94550

Sandia is a multiprogram laboratory operated by Sandia Corporation,
a Lockheed Martin Company, for the United States Department of Energy's
National Nuclear Security Administration under Contract DE-AC04-94AL85000.

Sandia National Laboratories

Issued by Sandia National Laboratories, operated for the United States Department of Energy by Sandia Corporation.

Available to DOE and DOE contractors from
U.S. Department of Energy
Office of Scientific and Technical Information
P.O. Box 62
Oak Ridge, TN 37831

Telephone: (865)576-8401
Facsimile: (865)576-5728
E-Mail: reports@adonis.osti.gov
Online ordering: http://www.doe.gov/bridge

Available to the public from
U.S. Department of Commerce
National Technical Information Service
5285 Port Royal Rd
Springfield, VA 22161

Telephone: (800)553-6847
Facsimile: (703)605-6900
E-Mail: orders@ntis.fedworld.gov
Online order: http://www.ntis.gov/help/ordermethods.asp?loc=7-4-0#online

SAND 2004-1059
Unlimited Release
Printed March 2004

Molecular Simulations of MEMS and Membrane Coatings (PECASE)

Turkan Aydogmus, Asad Javaid, and David M. Ford
Department of Chemical Engineering
Texas A&M University
College Station, TX 77843-3122

Abstract

The goal of this Laboratory Directed Research & Development (LDRD) effort was to design, synthesize, and evaluate organic-inorganic nanocomposite membranes for solubility-based separations, such as the removal of higher hydrocarbons from air streams, using experiment and theory. We synthesized membranes by depositing alkylchlorosilanes on the nanoporous surfaces of alumina substrates, using techniques from the self-assembled monolayer literature to control the microstructure. We measured the permeability of these membranes to different gas species, in order to evaluate their performance in solubility-based separations. Membrane design goals were met by manipulating the pore size, alkyl group size, and alkyl surface density. We employed molecular dynamics simulation to gain further understanding of the relationship between membrane microstructure and separation performance.

-This page intentionally left blank-

Contents

Figures

Tables

1. Introduction

1.1. Background

In this report, we describe our experimental and theoretical study of organic-inorganic composite membranes for solubility-based gas separations [1-3]. In our experimental work, we synthesize membranes by depositing alkylchlorosilanes on the nanoporous surfaces of alumina substrates, using techniques from the self-assembled monolayer (SAM) literature to control the microstructure. (Such SAMs are also used in microelectromechanical (MEMS) devices.) We measure the permeability of these membranes to different gas species, in order to evaluate their performance in solubility-based separations. In our theoretical work, we use molecular dynamics (MD) simulation to gain further understanding of the relationship between membrane microstructure and separation performance.

In solubility-based membrane separations [4], the goal is to preferentially permeate one of the species based on its greater solubility in the membrane material; this is in some sense the opposite of a diffusivity-based separation, in which the more mobile species is preferentially permeated. Solubility-based separation is especially useful in applications where a small amount of a heavy species is present in a light gas stream (e.g. removal of higher hydrocarbons from natural gas, removal of volatile organic compounds from air). The preferential permeation of the larger species in such applications translates to lower membrane surface area and lower operating costs. Polymeric membranes with relatively high permeabilities, such as those made from polydimethylsiloxane (PDMS) and related polymers [5, 6], are in commercial use for such applications [7].

An architecture in which small organic molecules are attached to the porous surfaces of an inorganic substrate is attractive for solubility-based gas separation membranes, since (in principle) there is independent control over both the chemistry and free volume of the modified pore spaces [1-3]. Our work in this area was originally inspired by the work of Paterson and colleagues, who published a series of papers on the surface modification of

inorganic membranes with organic groups [8-11]. They used several different organic precursors, including silicone oil, octadecyltrichlorosilane (OTS), and alkyl phosphonic acids. In all cases, they changed the surface functionality of the membranes, making them hydrophobic. In one case [11], Randon and Paterson attached C4 and C12 phosphonic acids to the surface of 5 nm alumina membranes; after repeated treatments with C12, they significantly increased propane/nitrogen selectivity, albeit with a loss in permeability. In a study that paralleled ours, McCarley and Way [12] employed OTS on alumina membranes and found significant enhancement of selectivity for heavier gases over lighter ones. Miller and Koros [13] employed a similar material architecture, but used fluorine-substituted organosilanes to make rigid surface phases suitable for diffusivity-based separation membranes. The surface modification of ceramic membranes with alkylsilanes [14-16] and alcohols [17] has been proposed for liquid-phase separations as well. Martin and co-workers have used self-assembled monolayers in gold-coated [18-20] and silica [21] micropores to make membranes for various applications. In related work, the grafting of polymers into the pores of ceramic [22-26] and porous polymer [27-29] substrates has also been pursued as a route to highly selective and permeable membranes. The placement of small organic molecules on the walls of porous adsorbents such as MCM-41 has also been the subject of much recent interest [30-34].

Our main objective in this work was to quantify the effects of pore size, organic group size, and organic surface density on the performance of a modified membrane in a prototype solubility-based separation.

1.2. Experiments

We chose alkylchlorosilanes on porous ceramic supports as the basis for our study, so that we might benefit from the vast literature on analogous nonporous systems. Organochlorosilanes have been widely used to form stable SAMs on a number of surfaces, including inorganic oxides [35]. Modification of a surface can be achieved either by exposing it directly to a silane vapor or by immersing it in a solution containing

the silane reagent [36]. While SAM-based technology is mature enough to be used in a variety of application areas, a detailed understanding of SAM structure and function is still being pursued in the literature. Of particular interest (especially for liquid-phase synthesis) is how SAM structure is affected by the synthesis variables, so that protocols with high reproducibility may be developed. A list of the most important variables would certainly include substrate surface chemistry (especially the availability and nature of adsorbed water) [37-41], silane chemistry (organic moiety [42, 43] and reactive functionality [37, 44-47]), and reaction conditions (solvent type, silane concentration, temperature, and immersion time) [48]. While a majority of the SAM literature has focused on silica substrates, other materials have been studied as well [44, 49-51].

We chose propane, methane, and nitrogen as our test gases and employed them at near-ambient conditions of pressure and temperature. Permselectivity for a higher molecular weight species over a lower, such as propane over nitrogen, is an indicator of solubility selectivity.

In our first set of experiments [1], we carried out surface modification of 5 nm and 12 nm alumina membranes using different alkyl trichlorosilanes with chain lengths ranging from C4 to C28. All of these chains were straight except for C28, which had a geminal branched structure. The purpose was to evaluate the roles of pore size and alkyl group length on the separation. In our next set of experiments, we employed C18 trichlorosilane on 5 nm alumina membranes prepared under different conditions of surface hydration. We also employed a C18 monochlorosilane on a normally hydrated The purpose of these experiments was to explore our ability to modify the surface coverage of the alkyl SAM and monitor its consequences on membrane permselectivity.

We employed several different experimental techniques to characterize the composition and microstructure of the composite membranes, including Xray photoelectron microscopy (XPS) and scanning electron microscopy (SEM).

1.3. Molecular simulations

Molecular simulation [52, 53] has become a powerful tool for elucidating transport mechanisms in microporous materials. In molecular simulation, a model system is built at the atomic level with prescribed potentials (the force-field) acting between the atoms. These interactions consist of site-site interactions, such as van der Waals dispersion and Coulombic forces, and intramolecular forces, such as chemical bonds, angle bending and dihedral torsional barriers. A solid matrix, such as a mesoporous material, can be modeled as a collection of atoms with prescribed positions. Properties of interest, both local and global, can be averaged over either a Monte Carlo or molecular dynamics trajectory. In our case, we are particularly interested in the diffusivity and solubility of different gas species (especially propane, nitrogen, and methane) in the composite materials; the permeability, which is a direct point of contact with the experiments, may be obtained as the product of diffusivity and solubility. Since our experimental systems are fairly unique, there is not much work in the simulation literature that is directly relevant to the problem; some work in modeling reversed-phase chromatography [54-60] provide good points of comparison, however.

While molecular models that correspond as closely as possible to the experiments will be used, the main goal of the molecular simulation work is not exact quantitative predictions of membrane performance. Rather, what we expect is that the simulations will provide semi-quantitative and qualitative guidance to help us interpret the experimental results and guide us in interpreting the effects of alkyl chain length, pore size, and surface density. For example, the simulation work could provide molecular-level insight as to the physics behind the shape of selectivity-permeability performance curves. Based on our past experience in the molecular simulation field, this is a realistic expectation.

2. Experiments

2.1. Procedures

2.1.1. Membrane synthesis

Membralox® membranes from US Filter Ceramic Membrane Products (DeLand, Florida), provided the starting point for this research. Each membrane consisted of a mesoporous γ-alumina layer deposited on the inside of a macroporous alumina support tube. We employed two different products, described as "5 nm" and "1000 Dalton cutoff" by US Filter. From our permeation results (described in section 2.2.1 below), we concluded that the "1000 Dalton cutoff" membranes had an average pore size of 12 nm; we will therefore refer to them as "12 nm" membranes. These membranes have been discussed in detail by Liu and co-workers who have described and characterized them in a two part series [61, 62]. The tubes were originally 25 cm long with an outer diameter of 1.0 cm and an inner diameter of 0.7 cm; for our experiments, we cut them into 1 inch long pieces using a laboratory glass cutter. The majority of the membrane thickness is comprised of extruded α-alumina with an average pore size of 10 μm. This macroporous support is coated by slip casting and firing two more layers of α-alumina with average pore diameters of 0.8 and 0.2 μm. The final layer, which is 3-5 μm thick, is γ-alumina that is slip-cast and fired to yield an average pore size of 5 (or 12) nm and a porosity of 50% [61]. Figure 1 is an SEM image of the membrane in cross-section; all three slip cast layers and a portion of the macroporous support (left) are shown.

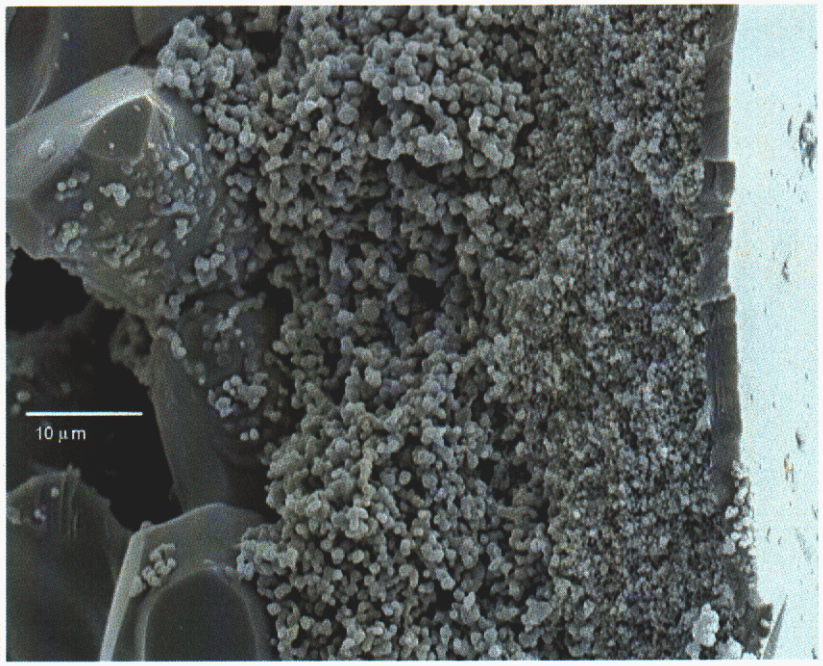

Figure 1. SEM image of a cross-section of a 5 nm alumina membrane, showing the configuration of the four layers.

After cutting, the membranes were soaked in a 2:1 ethanol/water mixture for 24 hours at ambient temperature (the ethanol was obtained from EM Science). The membranes were then dried in an oven at 60°C for 30 minutes and stored in a normal laboratory environment. As a baseline, permeance data were obtained for nitrogen, methane, and propane on the untreated membranes, according to the procedure described in section 2.1.2.

Membranes used without any further treatment were denoted as "normally hydrated," or NH. To create "dehydrated" membranes, denoted as DH, the membranes were dried in an oven at 180 °C under vacuum for 6 hours. They were then placed in a desiccator and allowed to come to room temperature; they were stored in the desiccator until treated with organochlorosilane. To obtain "superhydrated," or SH, membranes, the membrane pieces were boiled in distilled water for 10 hrs and dried in the laboratory environment. The protocols followed for dehydration and superhydration of membranes were slight

modifications of the procedures reported in the literature for dehydration and superhydration of silica wafers [39, 48].

The membranes were surface-derivatized using solutions of alkylchlorosilanes in toluene. Most were trichlorosilanes with carbon numbers ranging from C4 to C28 (e.g. octadecyltrichlorosilane - OTS). All of the chains were normal alkanes, except C28 which had a geminal branched structure. The monochlorosilane version of OTS, dimethyloctadecylchlorosilane (DMODCS), was also used in one set of experiments.

Solutions of single alkylchlorosilanes in toluene (0.05M) were made inside a glove box under nitrogen environment. The membrane piece to be treated was placed in a glass bottle in the glove box and the solution was added using a pipette. The membrane was soaked in the solution for 2 hr at ambient temperature, after which the membrane was removed and rinsed with toluene. The membrane was then taken out of the glove box and soaked for 24 hr in toluene to remove any excess (physisorbed) chains. The membrane was then soaked for another 24 hr in a 2:1 ethanol/water solution to wash away the toluene. Finally, the treated membranes were dried at 60 °C for 30 min. At least three different membrane pieces were used as replicates at a given treatment condition. The results from the different replicates were used to generate the standard deviations on the data presented here.

All alkylchlorosilane reagents were obtained from Gelest Inc (Tullytown PA). Anhydrous toluene was obtained from Aldrich and ethanol (for cleaning purposes) was obtained from EM Science. All reagents were used as obtained, without further purification. Instrument grade propane, methane, and nitrogen were obtained from Praxair.

2.1.2. Permeation measurements

In this report, we describe only pure gas permeation experiments. The tubular membrane piece was placed inside a cylindrical steel module with feed and retentate openings at either end and one permeate opening on the shell side. Rubber gaskets, tightened by

screw caps to ensure proper sealing of the tube side from the shell side, were used at both ends. A pure gas was delivered to the feed side at the desired pressure; the retentate exit was blocked, forcing all of the gas to flow across the membrane and through the permeate outlet (which was maintained at ambient pressure). The permeate flow was measured using a bubble flow meter. The pressure difference across the membrane, Δp, was measured using a digital pressure gauge. Volumetric flow rate was measured at four different values of Δp, ranging from 0.5 to 1.1 bars. Ambient pressure and temperature were monitored, and the volumetric flow rate was converted to molar flow rate assuming ideal gas behavior. For the data presented here, the ambient temperature ranged from 21 to 25 °C, while the ambient pressure ranged from 0.995 to 1.01 bar. The molar flux was calculated by dividing the molar flow rate by membrane flow area, which we determined to be 0.000559 m^2 for our membrane pieces. The molar fluxes were then plotted against Δp and the plots were observed to be linear, as might be expected for the relatively low feed pressures used here. The permeance of pure species i, P_i, was therefore obtained from a linear regression of the data. For a given gas pair, the permeance of each gas was measured individually and the ideal selectivity was found by dividing the respective permeances, e.g. as

$$\alpha_{propane/nitrogen} = \frac{P_{propane}}{P_{nitrogen}} \quad (1)$$

2.1.3. Materials characterization

After the permeation experiments, the membranes were characterized by XPS. For this purpose, the tubular membrane had to be split open to expose the inner surface, where the 5 nm γ-alumina layer is located. Most of the XPS work was carried out at Texas A&M using a Kratos analytical Axis His 165 instrument with monochromatic aluminum X-ray source and an electron flood gun for charge neutralization. Photo-electron peaks for carbon (C 1s), oxygen (O 1s), silicon (Si 2p) and aluminum (Al 2p) were collected.

In addition to XPS scans of the treated surface, as described above, we also wanted information on the the depth to which the organic coating penetrated the porous alumina

substrate. To obtain an elemental depth profile, periodic argon ion sputtering was performed on the surface analysis region to remove layers of material, and new XPS elemental spectra were gathered after each sputtering period. The etching depths were not measured directly on the sample, but are reported with respect to the known etching rate of a reference silica sample under the same conditions. This depth-profiling XPS work was carried out by Evans Texas (Round Rock, TX) using a Surface Science Instruments Model SSX-100 (101) instrument with a monochromatic aluminum X-ray source and an electron flood gun for charge neutralization. Photoelectron peaks for carbon (C 1s), oxygen (O 1s), silicon (Si 2p), and aluminum (Al 2p) were collected.

For some membrane pieces, SEM images were also taken; this was done using a JEOL JSM-6400 analytical-grade instrument, which had the added capability of conducting elemental analysis using the energy dispersive spectroscopy (EDS) system. To enable viewing of the membrane inner surface with SEM, the broken membrane pieces were covered with a very thin film of gold-palladium under vacuum.

2.2. Results

2.2.1. Baseline properties of untreated membranes

Bare membrane permeance data are given in Fig. 2. The average nitrogen permeance was $1.04 \pm 0.23 \times 10^{-5}$ mol sec^{-1} m^{-2} Pa^{-1} for 5 nm membranes and $1.88 \pm 0.113 \times 10^{-5}$ mol sec^{-1} m^{-2} Pa^{-1} for "1000 Dalton" membranes. These results are in very good agreement with the data provided by US Filter in which nitrogen permeance is given as $0.87 \pm 0.248 \times 10^{-5}$ mol sec^{-1} m^{-2} Pa^{-1} for 5 nm membranes and $1.86 \pm 0.22 \times 10^{-5}$ mol sec^{-1} m^{-2} Pa^{-1} for "1000 Dalton" membranes. Assuming that nitrogen transport is primarily via the Knudsen diffusion mechanism, and taking into account that the thickness of the mesoporous layer is 25% smaller for the "1000 Dalton" membranes [63], our data suggest that the average pore size for these membranes is about 12 nm.

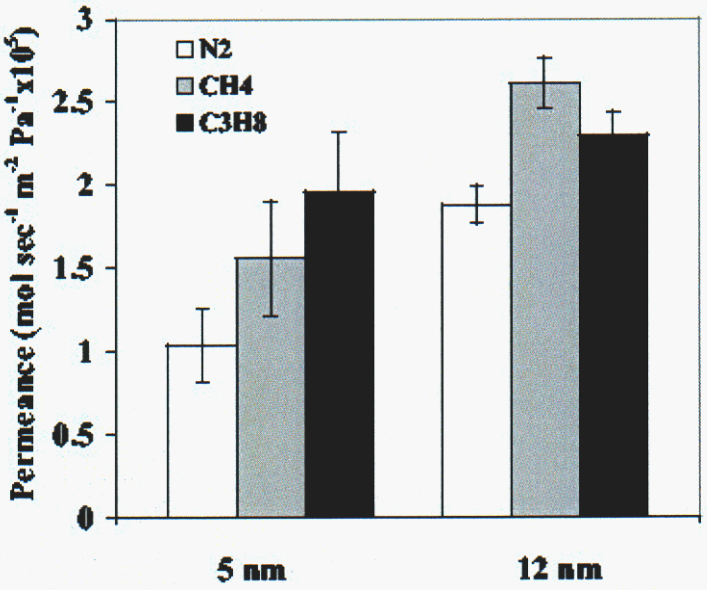

Figure 2. Bare membrane permeance data for 5 nm and 12 nm membranes.

Figure 3 shows a comparison of the selectivities for the bare 5 nm and 12 nm membranes. For the 5 nm membranes, the selectivity of methane over nitrogen was 1.5, which is very close to the square root of the inverse ratio of the molecular weights of methane and nitrogen (1.3). Furthermore, at 20 °C and a pressure of 2.1 bar, the mean free paths of nitrogen and methane are 47 and 38 nm respectively; these values are obviously larger than the nominal pore diameter. These results strongly suggest that Knudsen diffusion is the dominant mechanism of transport for nitrogen and methane in bare 5 nm membranes. However, the propane/methane selectivity of 1.28 and the propane/nitrogen selectivity of 1.91 are quite contrary to what a Knudsen separation mechanism would yield (less than unity in both cases). This suggests that surface adsorption and/or capillary condensation effects are significant for propane even in the bare 5 nm membranes, leading to a higher permeance for that gas.

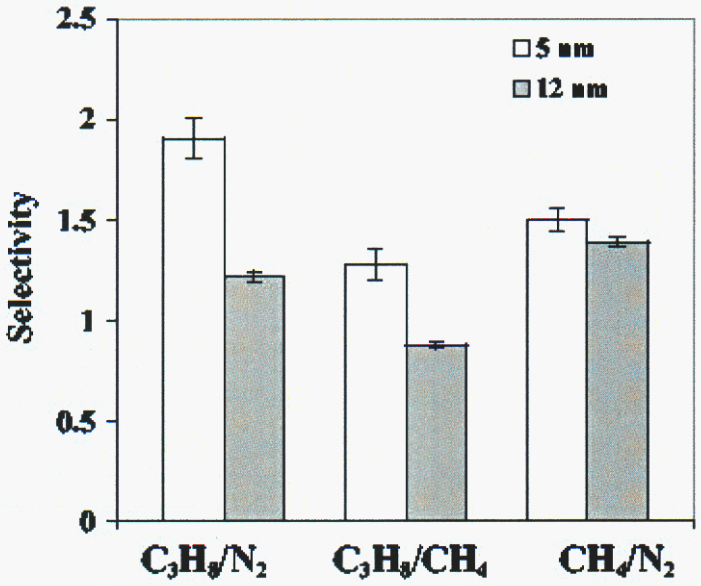

Figure 3. Comparison of propane/nitrogen, propane/methane and methane/nitrogen selectivities for bare 5 nm and 12 nm membranes.

For the 12 nm membranes, the methane/nitrogen selectivity was 1.39, again strongly suggesting the Knudsen mechanism of transport for those gases. Apparently the surface adsorption and condensation effects are smaller in the 12 nm membranes, because the propane/methane and propane/nitrogen selectivities were only 0.88 and 1.22, respectively. This is consistent with the 12 nm membranes having a larger average pore size than the 5 nm membranes, as indicated by the nitrogen permeance data.

2.2.2. Effects of alkyl chain length and pore size

All of the results in this section are for normally hydrated substrates treated with alkyltrichlorosilanes. The effect of chain length on the various selectivities in surface-modified 5 nm membranes is shown in Fig. 4. All treatments were carried out with the same concentration of the trichlorosilane reagent and for the same reaction time, as described above. It is quite evident that increasing the chain length increases the propane/nitrogen selectivity. For the C22 chain length, the selectivity was the highest and represented a 16-fold increase over that of the bare membrane. Although it appears that the results for C28 are anomalous, this alkyl group was a geminal branched chain with the longest branch being C14; a selectivity somewhere between that of the C12 and

C18 membranes is therefore not surprising. Propane/methane selectivity shows a significant improvement for C18, C22, and C28 chain lengths only, with a maximum value of 10 for the C22 chain length. No substantial improvement in the methane/nitrogen selectivity is evident after modification with any of the chlorosilanes.

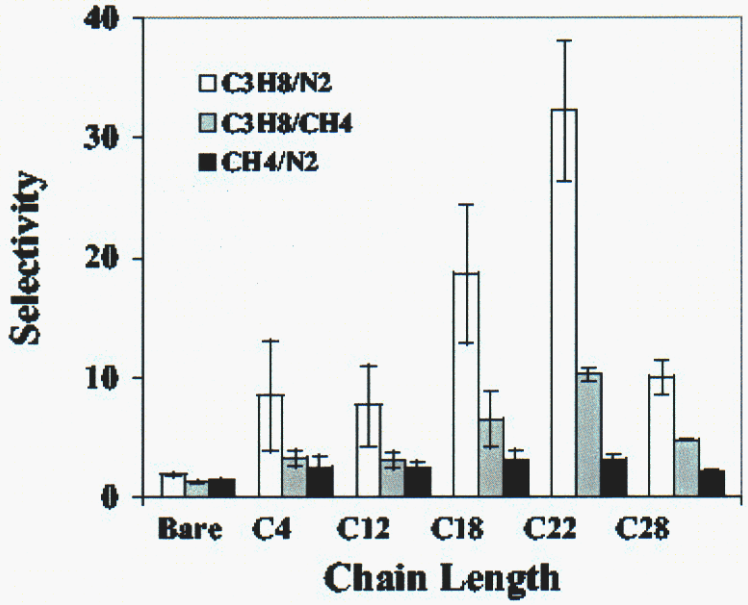

Figure 4. Effect of chain length on propane/nitrogen, propane/methane and methane/nitrogen selectivities for 5nm membranes.

In addition to selectivity, the permeance is a very important factor in measuring membrane performance. Figure 5 is a selectivity-permeance plot for propane/nitrogen separation on 5 nm membranes. The plot shows that propane permeance decreased by as much as 2 orders of magnitude upon surface modification, while selectivity increased significantly. Furthermore, the permeance and selectivity were correlated with the chain length used. Although the results for the shorter (C4 and C12) chains were statistically indistinguishable, the longer (C18 and C22) chains exhibited significantly better performance. In fact, increasing the chain length beyond C12 appears to greatly increase selectivity without much loss in permeability; this is of course a very desirable situation. Again, C28 shows results that are consistent with its branched structure. A data point from the literature [5] for a polydimethylsiloxane (PDMS) membrane is shown for comparison.

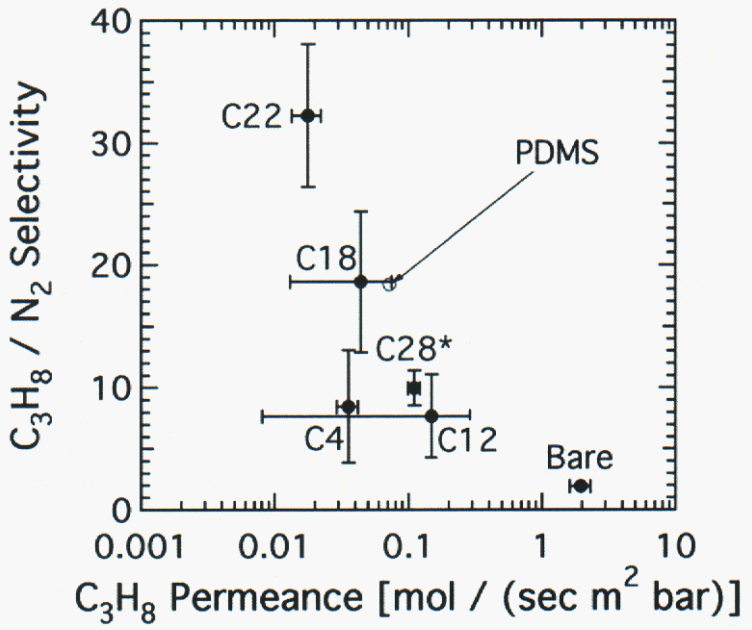

Figure 5. Propane/nitrogen selectivity as a function of propane permeance in 5 nm membranes.

Figure 6 summarizes the effects of pore size by comparing the performance of the 5 nm and 12 nm membranes for three different treatments (untreated, C12, and C18). The 5 nm substrates produce more selective and less permeable membranes for any given treatment, with the effects becoming more pronounced for the larger chain lengths.

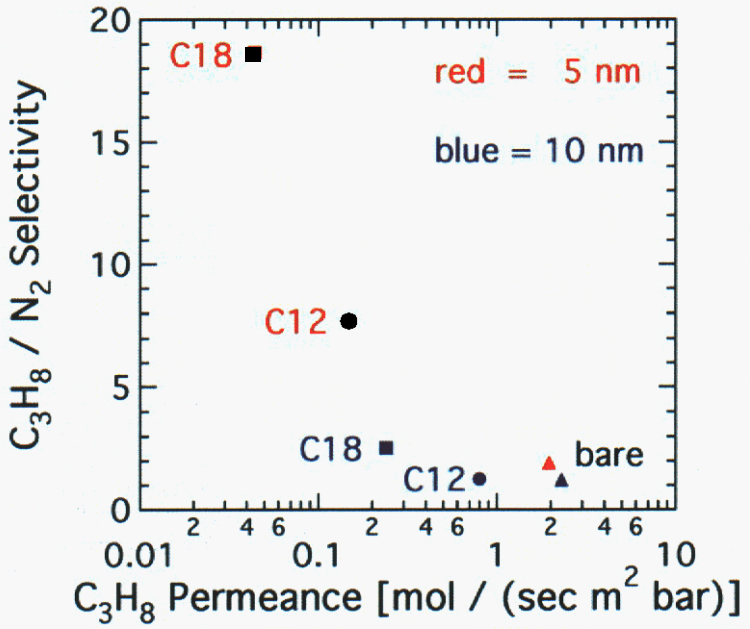

Figure 6. Comparison of performance in 5 nm and 12 nm membranes. The circles represents bare membranes, the squares represent membranes treated with C12 chains, and the diamonds represent membranes treated with C18 chains.

Results from the XPS depth profile analysis, as described in Section 2.1.3, are shown in Fig. 7. We focus on carbon and silicon, since these elements should indicate the presence of our surface-attached alkylsilanes. The molar percentage of carbon detected at the inner surface of the C18 treated membrane was about 70%, which is significantly higher than the 30% detected at the inner surface of the bare membrane. In both the treated and bare membranes, the molar percentage of carbon decayed to a nearly constant value by a depth of ~60 Å. We believe that the carbon on the bare membrane was adventitious in nature, or perhaps left over from the organics used in the washing process. Silicon was detected only in the C18 treated membrane, as expected. Interestingly, the molar percentage of silicon also decays quickly, falling below detection limits at a depth of ~40 Å.

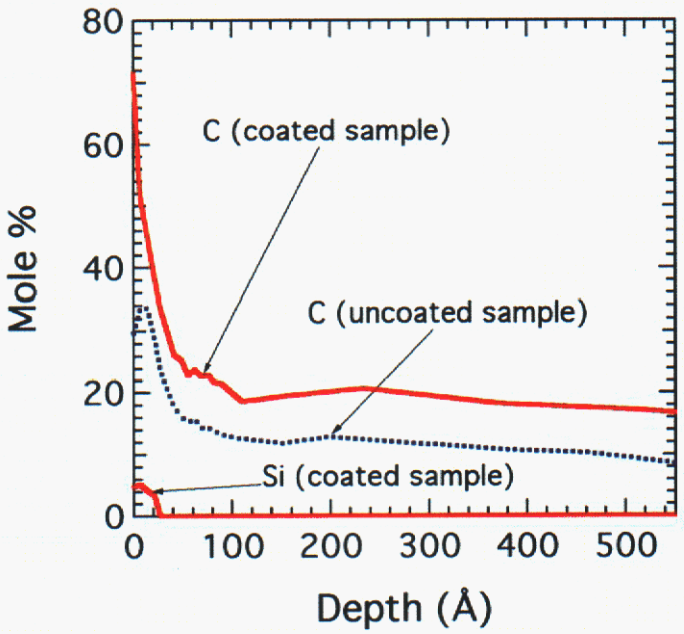

Figure 7. Molar percentage of elements detected by XPS as a function of depth from the inner surface of 5 nm membranes. The dashed line represents results from a bare membrane and the solid lines represent results from a membrane treated with C18 trichlorosilane. No silicon was detected on the bare membrane. Depth is reported with respect to a reference silica sample.

2.2.3. Effects of surface hydration and reactive functionality

All of the results in this section are for C18 alkyl groups. The hydration state of the alumina substrate prior to treatment was varied, as described in section 2.1.1. All but one of the experiments were done with the C18 trichlorosilane, OTS. One experiment, with a normally hydrated substrate, was done with the C18 monochlorosilane, DMODCS.

Propane and nitrogen permeance, ideal selectivity, and XPS elemental analysis data (from surface scan, not depth profiling) for the bare and OTS modified membranes are given in Table 1. The XPS data are reported in terms of molar percentage of carbon and silicon; the remainder of the XPS signal was from Al and O in the expected ratio.

Degree of hydration	Permeance (mol sec^{-1} m^{-2} bar^{-1}) C_3H_8	N_2	Selectivity C_3H_8/N_2	Carbon mol%	Silicon mol%
Bare	1.04 (0.18)	0.62 (0.087)	1.68 (0.12)	12.6 (2.7)	0.0
Normally hydrated	0.016 (0.0047)	0.0008 (0.0002)	19.9 (4.3)	73.4 (8.2)	5.1 (0.39)
Dehydrated	0.0097 (0.0056)	0.0023 (0.0016)	4.36 (0.45)	47.0 (9.3)	4.3 (1.3)
Superhydrated	0.68 (0.40)	0.52 (0.28)	1.23 (0.21)	68.0 (6.5)	6.5 (1.2)

Table 1. Propane and nitrogen permeance, ideal selectivity, and molar percentage of elements as detected by XPS, for bare and OTS-treated membranes. For the OTS-treated membranes, data are given for three different pretreatment hydration states, as discussed in the text. Standard deviations are given in parentheses.

The molar percentage of carbon detected on the surface of all modified membranes was significantly higher than that for the bare membrane. The theoretically expected C/Si ratio for all OTS treated membranes was 18. While experimental C/Si ratios greater than the theoretical value are common with XPS, due to screening effects from the monolayer geometry [51] or the presence of adventitious carbon [64], our data consistently reflected C/Si ratios lower than the theoretical: 14.4, 11.0, and 10.4 for the NH, DH, and SH membranes respectively. We are not currently able to explain this finding; it may be related to the rough, nanoporous geometry of the alumina substrate.

The NH membranes exhibited the highest propane/nitrogen selectivity and also the highest carbon content. The selectivity for the DH membranes was significantly lower than the selectivity shown by the NH membranes, due to a combination of factors; the propane permeance for the DH membranes was about 40% smaller than that for the NH, while the nitrogen permeance was a factor of 3 higher. The XPS characterization experiments showed a significantly lower carbon content for the DH membranes, as compared to the NH membranes. We believe that the permeance data for the DH membranes also suggest a lower surface chain density, based on the following rationale. A lower surface coverage could be expected to result in both an increased diffusivity (higher free volume) and a decreased solubility (fewer van der Waals interactions); the former effect would tend to increase the permeance while the latter would tend to

decrease it. Furthermore, the relative importance of these two effects would depend on the gas species; one might expect a lighter molecule to be more affected by the increased diffusivity, while a heavier molecule would be more affected by the decreased solubility. Our data are consistent with this hypothesis; the DH membranes have a nitrogen permeance that is nearly a factor of 3 higher, and a propane permeance that is 40% lower, as compared to the NH membranes. Of course, our findings are also consistent with our general expectations from the literature [37-41], where it has been well established that SAMs formed on the surface of a dehydrated inorganic substrate are less dense than those formed on a well hydrated surface.

The SH membranes showed no increase in selectivity as compared to bare membranes; the individual propane and nitrogen permeances were comparable to those of the bare membranes. Interestingly, however, the carbon mol% detected on the surface of the SH membranes was statistically similar to that observed in the NH membranes. Thus, the permselectivity and XPS surface analysis results for the SH membranes were apparently contradictory to each other. To obtain a better understanding of this behavior, we observed the inner surfaces of the NH and SH membranes with SEM.

Figure 8 is an SEM image of the inner surface of an untreated membrane and Figure 9 is an SEM image of the inner surface of a treated (NH) membrane. One interesting observation about both Figures is the presence of defects, in which the active layer has detached from the macroporous support over a scale of 10-100 μm. While the overall defect surface coverage was not as high as implied by these images (which focus on them), it was higher than that normally considered for pinhole defects in such membranes [65-67]. However, we did not find any evidence of defects in the gas permeation measurements before or after treatment, contrary to some previous research [65]. We also note that the concentration of surface defects observed in the SEM images was not correlated with the presence or absence of treatment with OTS. Based on these considerations, we conclude that most of the defects were created (or exacerbated) while preparing the samples for SEM imaging.

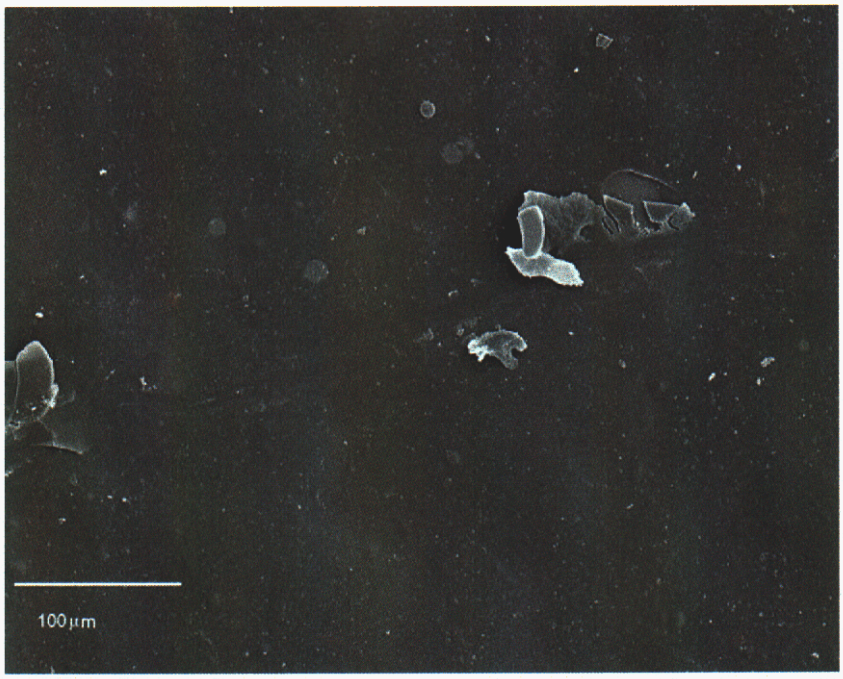

Figure 8. SEM of the inner surface of an untreated 5 nm membrane.

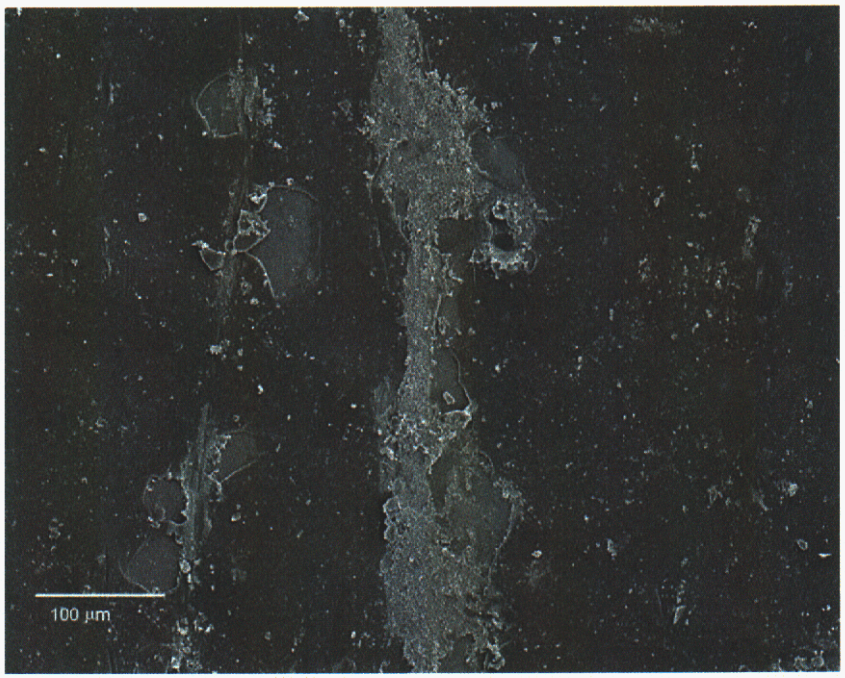

Figure 9. SEM of the inner surface of a "normally hydrated" membrane modified with OTS.

Another important observation from Figs. 8 and 9 is that the NH membrane looks no different than the bare membrane. Presumably, the SAM film is too thin to be detected by SEM for the NH case.

Figures 10 and 11 are images of the inner surface of an SH membrane at 230x and 600x magnification, respectively. In comparison to the NH membrane, the SH membrane surface shows visible evidence of the formation of a surface film, with considerable cracking. Elemental analysis conducted using the EDS system showed a high degree of carbon and silicon content present in this film, thus confirming the XPS findings. The evidence suggests that the OTS, due to the presence of excess moisture in the SH substrates, polymerized into a (relatively) thick film instead of forming a monolayer, or small number of multilayers, at the surface. The resultant film suffered significant cracking during the post-treatment drying process, leaving large gaps for essentially free gas transport. This explains why we detected a significant amount of carbon and silicon on the SH membrane surface but did not observe any significant drop in permeance of either gas as compared to the bare membrane.

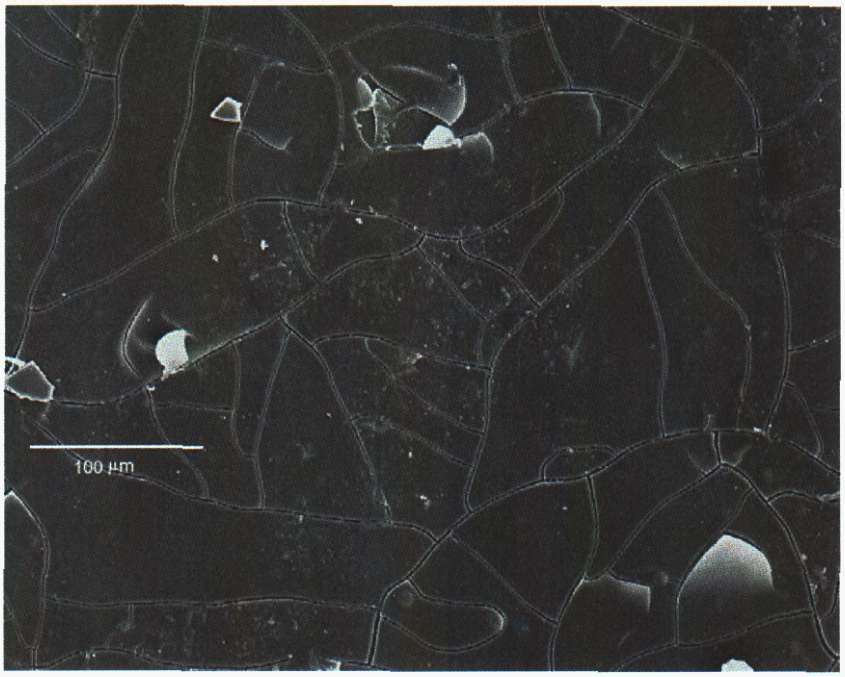

Figure 10. SEM of the inner surface of a "superhydrated" membrane modified with OTS.

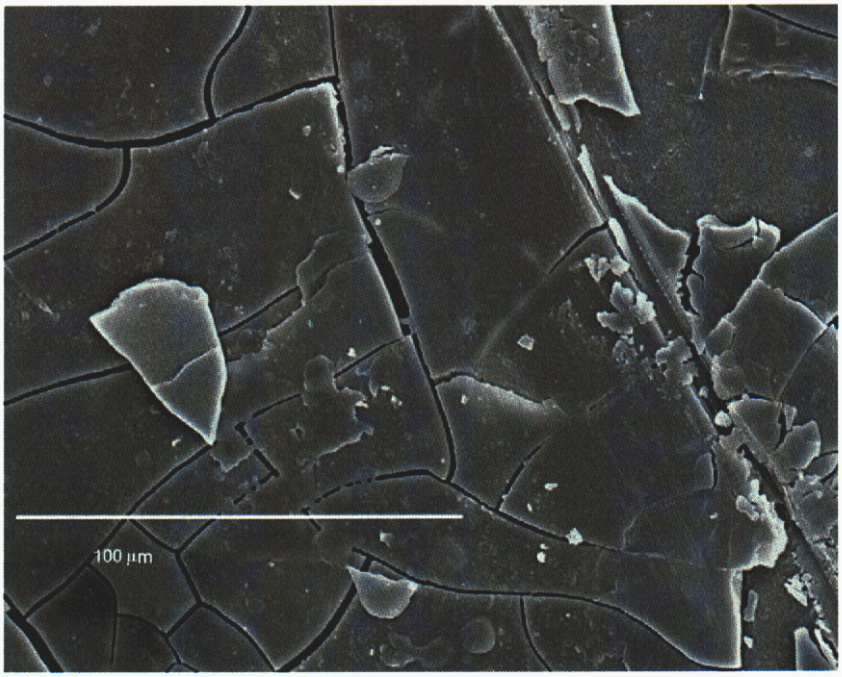

Figure 11. Another SEM of the inner surface of a "superhydrated" membrane modified with OTS, at higher magnification.

We were not able to achieve any detectable organosilane attachment with the mono-functional reaction chemistry (DMODCS), according to both XPS and permselectivity data. This was somewhat surprising; based on the silica SAM literature, we expected a reduced, but detectable, surface coverage as compared to the tri-functional reagents. However, in their study of OTS and DMODCS monolayers on alumina, Thompson and Pemberton [44] needed integration times more than 20x longer for DMODCS to obtain Raman spectra of comparable intensity. If the surface concentration of DMODCS was indeed more than an order of magnitude smaller than that of OTS in our systems, it is reasonable to expect that we would not detect it by XPS or permeation. Furthermore, Alami-Younssi et al. [15] recently reported that they were unable to detect any deposition of TMCS (C1 monochlorosilane) on alumina membranes or powders, under conditions where di- and tri-functional chlorosilanes and alkoxysilanes were readily grafted.

It is likely that multilayered polymeric networks were formed off of the surface during treatment with the trifunctional silanes. The SH membranes clearly had a thick film of polymerized OTS at the surface. Furthermore, the NH membranes created from OTS had percentages of surface carbon and silicon that were statistically similar to those from the

SH membranes. Therefore, it is not unreasonable to assume that the NH membranes were comprised of polymerized films of lesser thickness. Since we obtained no detectable coverage with the monofunctional silane, it is unfortunately not possible at this time to make a meaningful comparison with analogous systems that are guaranteed not to polymerize.

We still do not have a good understanding of the interplay between the network formed by the trifunctional silanes and the underlying pore structure. Some outstanding issues include the ability of the surface film to span pore openings, penetrate into the pore interiors, and heal pinhole defects. Our characterization using XPS with argon ion sputtering (end of section 2.2.2) has indicated that the deposited OTS is primarily localized within a few nanometers of the outer surface of 5 nm alumina substrates. In an interesting recent study on alumina/titania membranes modified with alkyldichlorosilanes [16], Van Gestel et al. used liquid (hexane, water) permeability as a probe that is sensitive to the surface chemistry throughout the interior of the porous structure. They concluded that C1 and C8 dichlorosilanes were able to access the interiors of mesoporous structures (pore size ≥ 2 nm) but formed primarily surface films on substrates with smaller pores.

2.3. Conclusions

Clearly we were able to modify the character of the alumina surface and change the transport mechanisms from Knudsen and surface-flow to solution-diffusion. Generally, the results followed trends that might be expected. As the pore size was decreased or the oligomer length was increased, the permeance became smaller and the selectivity for the heavier organic species became greater. Our most propane-selective membrane was produced from the longest chains (C22) and the substrate with the smallest pore size (5 nm). Freeman and Pinnau [4] have discussed the possibility of obtaining positive correlations between selectivity and permeability when designing materials for solubility-based separations. Although this does not seem to be the case for the systems studied here, it was encouraging to note that as we increased the chain size to C18 and C22 in the

5 nm membranes, we were able to enhance selectivity without much loss in permeability (see Fig. 5).

The XPS characterization experiments confirmed and clarified our conceptual picture of the structure of these composite membranes. The carbon and silicon content in the treated membranes confirmed that our synthesis procedure resulted in the deposition of alkylsilanes. Furthermore, the changes in the carbon and silicon signals with depth suggested that the organic coating was most dense at the surface and monotonically decayed to nearly zero density over the first few nanometers of the mesoporous substrate.

The effect of synthesis variables on the formation of surface-derivatized porous membranes using organosilane chemistry was investigated, by carrying out surface treatments with different alkylchlorosilane molecules under varying hydration states of the inorganic substrate. With regards to surface hydration, the "normally hydrated" membranes showed the best results. Significantly lower attachment of the organosilanes occurred with the "dehydrated" membranes. In the case of "superhydrated" membranes, polymerization of the trichlorosilane due to the presence of excess moisture led to the development of a thick, highly defective surface film. Modifications of the inorganic substrate with a monochlorosilane did not result in any significant attachment of the organic molecules to the membrane surface, in contrast to the trichlorosilanes.

3. Molecular simulation

3.1. Methodology

3.1.1. Molecular models

Figure 12 shows a schematic of the basic molecular-level model.

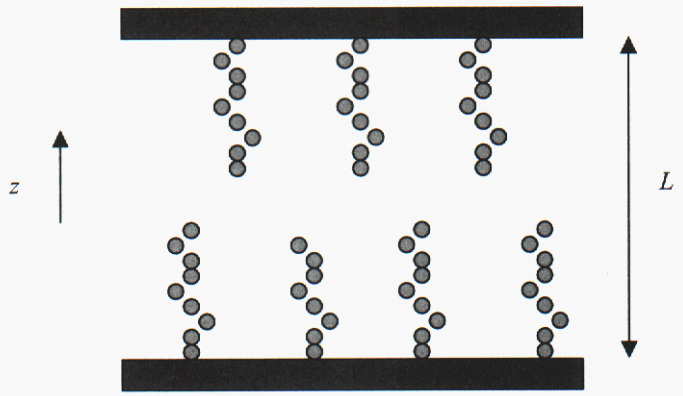

Figure 12. Two-dimensional representation of a model slit pore (actual model was three-dimensional). The pore contains a set of deposited alkylsilane molecules tethered to the alumina surface at a fixed coverage. Periodic boundary conditions are employed in the x and y directions (parallel to the pore walls).

The alumina surfaces were represented as featureless walls using the approach of Steele [68]. The pores of the alumina membranes are known to be slit-shaped, so this is an appropriate model. We considered values of the pore size L ranging from ~30 Å to ~100 Å, as indicated by the experimental information on pore sizes in the bare membranes. We used surface densities of 2 μmol/m^2 and 4 μmol/m^2 for the alkylsilane chains.

The chains were fixed to the walls with simple harmonic springs. The first monomer of a chain was randomly tethered to the wall within the distance of 3 ± 1.5 Å to capture surface roughness effects. Initial configurations were created with a stochastic builder based on the rotational isometric states (RIS) method [69]. For simplicity, we modeled the alkyl segments using the united-atom approach [48] where (-CH_2-) and (-CH_3-) segments were considered as one single site. Bond-stretching, angle-bending, and torsional potentials were applied to the chain segments. Specifically, we modeled octyl (C8), dodecyl (C12) and octadecyl (C18) chains. The model penetrants were nitrogen and propane, as used in the experiments; they were also modeled by using the united-atom approach. The non-bonded interactions were modeled by the 12-6 Lennard Jones (LJ) potential. Potential models were taken from sources in the literature [60, 70-72]. The temperature of interest was 298 K, corresponding to the experimental temperatures.

3.1.2. Property prediction

Our main molecular simulation technique was canonical molecular dynamics (MD) [52, 53]. All of our properties were calculated at infinite dilution of the gas (penetrant) species in the membrane (i.e. the Henry's Law limit). The diffusivity of each penetrant species was estimated by measuring ensemble-averaged mean-squared displacement as a function of time [73]. The solubility of each penetrant species was obtained using the Widom insertion method [72, 74].

Molecular simulation gives us the solubility, diffusivity, and permeability of the penetrants in a given model pore. The corresponding macroscopic properties of the membrane can be predicted either by straightforward integration of these properties over the pore size distribution or by the use of more rigorous lattice methods [75]. For the purposes of this work, we assumed a very narrow (i.e. delta function) pore size distribution function centered at the pore size of the model.

In addition to predictions of macroscopic properties, local profiles of properties across the width of the pore were also obtained [76], providing connections between the molecular-level behavior and the macroscopic properties. We generated density profiles for chain segments, and diffusivity and solubility profiles for penetrants. The density profiles produced by dividing the pore into bins parallel to the pore walls, and calculating the number of the chain segments in each bin periodically as simulation progressed. The bin widths were taken to be 0.2 and 0.33 Å for 30 and 50 Å pore sizes, respectively.

3.2. Results

The simulation results for the propane/nitrogen selectivity vs propane permeance for different chain lengths in two different pore-sized membranes are shown in Fig. 13. This plot may be compared with the experimental plots in Figs. 5 and 6 above. Because of the approximations in our model system, we don't see perfect quantitative agreement. However, we do have qualitative agreement with the experimentally observed trends.

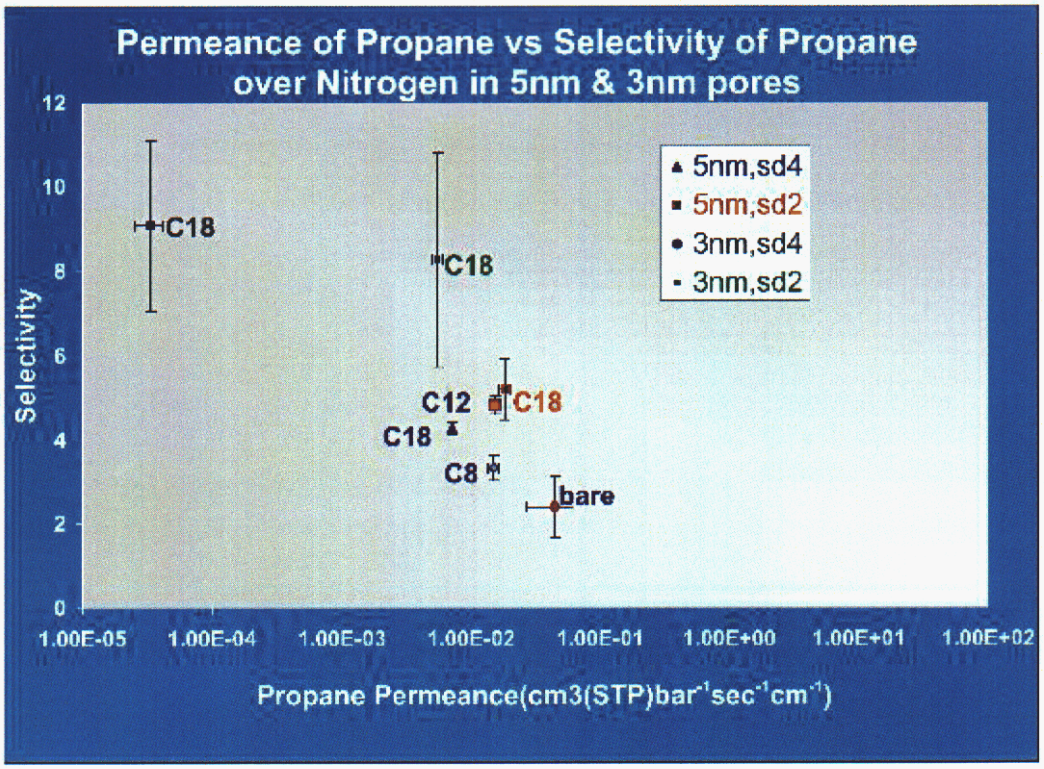

Figure 13. Selectivity-permeability plot for propane/nitrogen from molecular simulations.

The most obvious common feature between the experimental and simulation data is that the introduction of attached chains results in increased selectivity and decreased permeability. Furthermore, if we focus on the chain length effect, we see that the selectivity is enhanced as the chain length is increased. However, in the simulation results, the differences in the overall selectivity are not very clear. That is a consequence of the fact that the C18 alkyl-chains do not span the 5nm-pore completely. If we had produced data with even longer chains attached to the pore, we would probably have seen more clear selectivity differences between the different chain lengths.

There is also an interesting parallel between experiment and simulation in the effects of pore size. In the simulations, the larger (5 nm) pore has generally lower selectivities and less sensitivity to chain length than the smaller (3 nm) pore. This is also true for the experimental results in Fig.6, although the "large" and "small" pore sizes were 5 nm and 12 nm, respectively. This quantitative discrepancy may be due to inaccuracies in the

experimental pore size estimation. For example, the nominal 5 nm substrates actually contain a significant fraction of pores smaller than 5 nm [77], which may be controlling transport. Another possible explanation is the ability of the trifunctional chlorosilanes to form polymeric networks and bridge across pores even larger than 5 nm (a phenomenon that was not captured in the molecular models).

Another parameter of interest is the surface coverage. In the simulations, decreasing the surface coverage resulted in a significant increase of propane permeance and a small increase in the selectivity. The lower surface coverage allowed both penetrants to diffuse faster in the pore, to roughly the same degree. This result was not reflected in any of the experimental results. In the experiments, lower surface coverage (obtained in the case of a dehydrated surface prior to treatment) caused a significant decrease in the selectivity and little change in propane permeance.

We can also examine the individual components, diffusivity and solubility, that contribute to the permeability. Table 2 gives detailed data for the solubility and diffusivity of each penetrant in the various models.

Chain Length	Pore Size (nm)	Surface Density ($\mu mol/m^2$)	Gas Species	D (x 10^2) ($cm^2 sec^{-1}$)	α_D (D_P/D_N)	S [cm^3(STP) cm^{-3} bar^{-1}]	α_S (S_P/S_N)	P [cm^3 (STP) cm^{-1} bar^{-1} sec^{-1}]	α_P
BARE	5	-	Propane	1.27	0.7110	3.4927	3.3565	0.0442	2.3866
			Nitrogen	1.78		1.0406			
C8	5	4	Propane	0.204	0.4339	7.3655	7.6792	0.0150	3.3321
			Nitrogen	0.469		0.9591			
C12	5	4	Propane	0.155	0.4492	9.8899	10.7473	0.0154	4.8280
			Nitrogen	0.346		0.9202			
C18	5	4	Propane	0.0762	0.3654	9.4104	11.6854	0.0072	4.2697
			Nitrogen	0.209		0.8053			
C18	5	2	Propane	0.1320	0.4114	13.9950	12.6434	0.0184	5.2014
			Nitrogen	0.320		1.1069			
C18	3	4	Propane	0.000434	0.2782	7.7968	32.6389	0.00003384	9.0798
			Nitrogen	0.00156		0.2388			
C18	3	2	Propane	0.0199	0.3778	27.8693	21.8957	0.0055421	8.2717
			Nitrogen	0.0526		1.2728			

Table 2. Summary of diffusivity, solubility, and permeability data from the simulations.

This table supports the idea that we increased the solubility of the propane and decrease the diffusivity of both penetrants, upon adding chains. In the larger pore (5nm), the reduction of the diffusivity of the propane is much higher than that for nitrogen , which leads to a lower diffusivity selectivity. This counterbalances the effect of increasing the solubility of the propane and results in insignificant improvement in the overall selectivity. On the other hand, in the smaller pore, the increase in the solubility selectivity was much higher and more than enough to compensate for the decrease in the diffusivity selectivity. Lowering the surface density helped the process in the positive direction by not only increasing the diffusion of the propane molecules (with that also permeances), but also maintaining the diffusivity selectivity around the same value as in the 4 mmol/m2 case. By looking at the overall table, we can conclude that, in the 3 nm pore membrane, we filled the pore or closed the pore mouths by attaching the C18 alkyl

chains. Hence, we helped the separation process to change in the favor of the more soluble molecule, which is the propane in this case.

In order to get a further molecular level understanding, we analyzed the density profiles of the chains along the pore and the corresponding solubility profiles of the penetrants. The density profiles for the different chain lengths and pore sizes (not shown) supported the conclusion that the chains spanned the entire pore width only in the case of the longest chains (C18) and the smallest pore (3 nm). This is also reflected in the solubility profiles shown in Figure 14. The profiles indicate why the solubility-selectivity was so high for the C18 chains in 3 nm pores (Table 2).

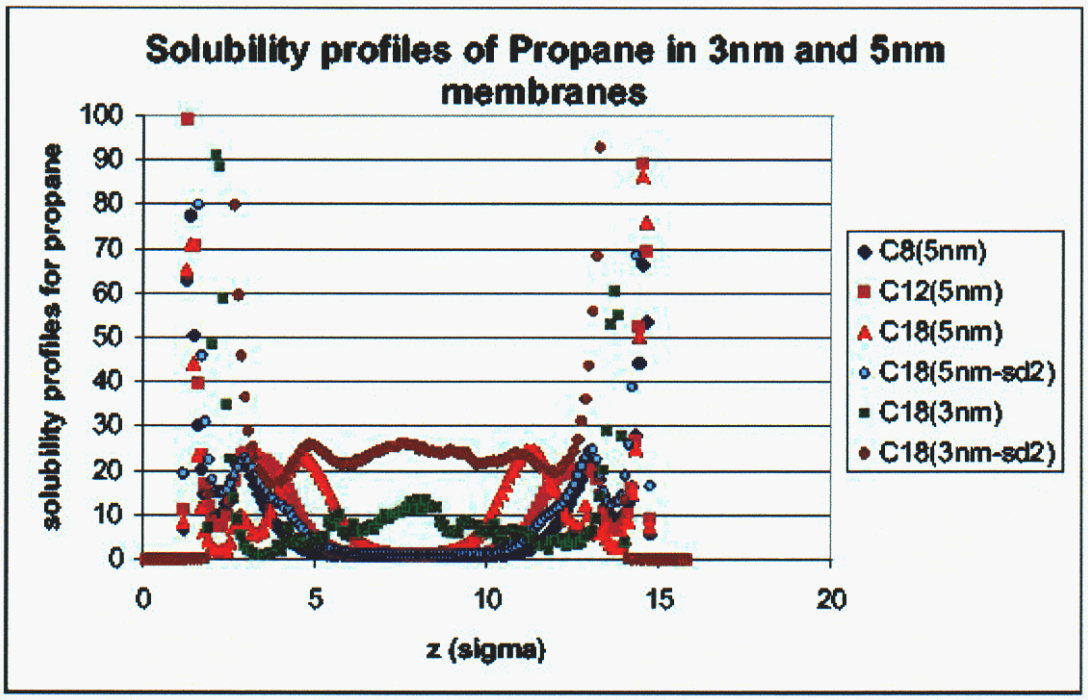

Figure 14. Solubility profiles of propane in models with various pore sizes, chain lengths, and densities.

3.3. Conclusions

We achieved good qualitative agreement with experiment in several respects, including the improvement in the overall selectivity of the membrane and decrease in the

permeance when increasing the chain length and pore size. Conditions under which chains span the pore yield the best improvement in the overall solubility selectivity, However, if the system is filled at too high a surface density with the alkyl chains, the permeance of the penetrants will drop significantly. In order to avoid that, one can find the best surface coverage by calculating the selectivity vs surface coverage profiles.

4. Summary

We synthesized composite membranes by decorating the surfaces of commercially available mesoporous alumina substrates with alkylchlorosilane self-assembled monolayers (SAMs), similar to those used in MEMS technology. We compared membrane performance to a benchmark polymeric material (polydimethylsiloxane, PDMS) for the removal of higher hydrocarbons from light gas streams. The deposited alkylchlorosilanes formed ultrathin (~10 nm) films that were located primarily on the substrate surface but penetrated a few nanometers into the pores. We were able to control the density of the film by manipulating the hydration state of the surface and choosing the reaction functionality of the silane. Furthermore, the density and chemical structure of the film strongly influenced the membrane permselectivity. Molecular simulation provided further insight into the structure-property relationships.

References

[1] A. Javaid, M.P. Hughey, V. Varutbangkul, and D.M. Ford, Solubility-based gas separation with oligomer-modified inorganic membranes, J. Membrane Sci. 187 (2001) 141-150.

[2] A. Javaid and D.M. Ford, Solubility-based gas separation with oligomer-modified inorganic membranes. Part II. Mixed gas permeation of 5 nm alumina membranes modified with octadecyltrichlorosilane, J. Membrane Sci. 215 (2003) 157-168.

[3] A. Javaid, D.A. Krapchetov, and D.M. Ford, Solubility-based gas separation with oligomer-modified inorganic membranes. Part III. Effects of synthesis conditions, J. Membrane Sci. submitted (2004).

[4] B. Freeman and I. Pinnau, Separation of Gases using Solubility-selective Polymers, Trends in Polymer Science 5 (1997) 167-173.

[5] S.A. Stern, V.M. Shah, and B.J. Hardy, Structure-Permeability Relationships in Silicone Polymers, Journal of Polymer Science: Part B: Polymer Physics 25 (1987) 1263.

[6] J. Schultz and K.-V. Peinemann, Membranes for separation of higher hydrocarbons from methane, J. Membrane Sci. 110 (1996) 37-45.

[7] M. Leemann, G. Eigenberger, and H. Strathmann, Vapour permeation for the recovery of organic solvents from waste air streams: separation capacities and process optimization, J. Membrane Sci. 113 (1996) 313-322.

[8] J. Randon, P. Blanc, and R. Paterson, Modification of ceramic membrane surfaces using phosphoric acid and alkyl phosphonic acids and its effects on ultrafiltration of BSA protein, J. Membrane Sci. 98 (1995) 119-129.

[9] C. Leger, H.D.L. Lira, and R. Paterson, Preparation and properties of surface modified ceramic membranes. Part II. Gas and liquid permeabilities of 5 nm alumina membranes modified by a monolayer of bound polydimethylsiloxane (PDMS) silicone oil, J. Membrane Sci. 120 (1996) 135-146.

[10] C. Leger, H.D.L. Lira, and R. Paterson, Preparation and properties of surface modified ceramic membranes. Part III. Gas permeation of 5 nm alumina membranes modified by trichloro-octadecylsilane, J. Membrane Sci. 120 (1996) 187-195.

[11] J. Randon and R. Paterson, Preliminary studies on the potential for gas separation by mesoporous ceramic oxide membranes surface modified by alkyl phosphonic acids, J. Membrane Sci. 134 (1997) 219-223.

[12] K.C. McCarley and J.D. Way, Development of a model surface flow membrane by modification of porous gamma-alumina with octadecyltrichlorosilane, Separation and Purification Technology 25 (2001) 195-210.

[13] J.R. Miller and W.J. Koros, The Formation of Chemically Modified γ-Alumina Microporous Membranes, Sep. Sci. Technol. 25 (1990) 1257-1280.

[14] S. Alami-Younssi, C. Kiefer, A. Larbot, M. Persin, and J. Sarrazin, Grafting γ alumina microporous membranes by organosilanes: Characterisation by pervaporation, J. Membrane Sci. 143 (1998) 27-36.

[15] S.A. Younssi, A. Iraqi, M. Rafiq, M. Persin, A. Larbot, and J. Sarrazin, gamma alumina membranes grafting by organosilanes and its application to the separation of solvent mixtures by pervaporation, Separation and Purification Technology 32 (2003) 175-179.

[16] T. Van Gestel, B. Van der Bruggen, A. Buekenhoudt, C. Dotremont, J. Luyten, C. Vandecasteele, and G. Maes, Surface modification of y-Al2O3/TiO2 multilayer membranes for applications in non-polar organic solvents, Journal of Membrane Science 224 (2003) 3-10.

[17] A. Dafinov, R. Garcia-Valls, and J. Font, Modification of ceramic membranes by alcohol adsorption, Journal of Membrane Science 196 (2002) 69-77.

[18] J.C. Hulteen, K.B. Jirage, and C.R. Martin, Introducing chemical transport selectivity into gold nanotubule membranes, Journal of the American Chemical Society 120 (1998) 6603-6604.

[19] K.B. Jirage, J.C. Hulteen, and C.R. Martin, Effect of thiol chemisorption on the transport properties of gold nanotubule membranes, Analytical Chemistry 71 (1999) 4913-4918.

[20] S.B. Lee and C.R. Martin, Controlling the transport properties of gold nanotubule membranes using chemisorbed thiols, Chemistry of Materials 13 (2001) 3236-3244.

[21] S.B. Lee, D.T. Mitchell, L. Trofin, T.K. Nevanen, H. Soderlund, and C.R. Martin, Antibody-Based Bio-Nanotube Membranes for Enantiomeric Drug Separations, Science 2002 (2002) 2198-2200.

[22] R.P. Castro, Y. Cohen, and H.G. Monbouquette, The permeability behavior of polyvinylpyrrolidone-modified porous silica membranes, J. Membrane Sci. 84 (1993) 151-160.

[23] C. Liu, W.J. Chen, and C.R. Martin, Electrochemical Synthesis of Ultrathin Film Composite Membranes, Journal of Membrane Science 65 (1992) 113-128.

[24] M. Nagale, B.Y. Kim, and M.L. Bruening, Ultrathin, hyperbranched poly(acrylic acid) membranes on porous alumina supports, Journal of the American Chemical Society 122 (2000) 11670-11678.

[25] K.P. Xiao, J.J. Harris, A. Park, C.M. Martin, V. Pradeep, and M.L. Bruening, Formation of ultrathin, defect-free membranes by grafting of poly(acrylic acid) onto layered polyelectrolyte films, Langmuir 17 (2001) 8236-8241.

[26] C. Liu and C.R. Martin, Composite Membranes from Photochemical-Synthesis of Ultrathin Polymer-Films, Nature 352 (1991) 50-52.

[27] H. Wang, K. Tanaka, H. Kita, and K. Okamoto, Pervaporation of aromatic/non-aromatic hydrocarbon mixtures through plasma-grafted membranes, J. Membrane Sci. 154 (1999) 221-228.

[28] T. Yamaguchi, T. Suzuki, T. Kai, and S. Nakao, Hollow-fiber-type pore-filling membranes made by plasma-graft polymerization for the removal of chlorinated organics from water, J. Membrane Sci. 194 (2001) 217-228.

[29] H. Yanagishita, D. Kitamoto, T. Ikegami, H. Negishi, A. Endo, K. Haraya, T. Nakane, N. Hanai, J. Arai, H. Matsuda, Y. Idemoto, and N. Koura, Preparation of photo-induced graft filling polymerized membranes for pervaporation using polyimide with benzophenone structure, J. Membrane Sci. 203 (2002) 191-199.

[30] C.P. Jaroniec, M. Kruk, M. Jaroniec, and A. Sayari, Tailoring Surface and Structural Properties of MCM-41 Silicas by Bonding Organosilanes, J. Phys. Chem. B 102 (1998) 5503-5510.
[31] C.E. Fowler, S.L. Burkett, and S. Mann, Synthesis and characterization of ordered organo-silica-surfactant mesophases with functionalized MCM-41-type architecture, Chem. Commun. 1997 (1997) 1769-1770.
[32] D.J. Macquarrie, D.B. Jackson, J.E.G. Mdoe, and J.H. Clark, Organomodified hexagonal mesoporous silicates, New J. Chem. 23 (1999) 539-544.
[33] X. Feng, G.E. Fryxell, L.-Q. Wang, A.Y. Kim, J. Liu, and K.M. Kemner, Functionalized Monolayers on Ordered Mesoporous Supports, Science 276 (1997) 923-926.
[34] L. Mercier and T.J. Pinnavaia, Access in Mesoporous Materials: Advantages of a Uniform Pore Structure in the Design of a Heavy Metal Ion Adsorbent for Environmental Remediation, Adv. Mater. 9 (1997) 500-503.
[35] J. Sagiv, Organized monolayers by adsorption. 1. Formation and structure of oleophobic mixed monolayers on solid surfaces, J. Am. Chem. Soc 102 (1980) 92-98.
[36] E.F. Vansant, P. Van der Voort, and K.C. Vrancken, eds. *Characterization and Chemical Modification of the Silica Surface*. Studies in Surface Science and Catalysis. Vol. 93. 1995, Elsevier: Amsterdam.
[37] D.L. Angst and G.W. Simmons, Moisture absorption characteristics of organosiloxane self-assembled monolayers, Langmuir 7 (1991) 2236-2242.
[38] P. Silberzan, L. Leger, D. Ausserre, and J.J. Benattar, Silanation of silica surfaces. A new method of constructing pure or mixed monolayers, Langmuir 7 (1991) 1647-1651.
[39] C.P. Tripp and M.L. Hair, Reaction of alkylchlorosilane with silica at the solid/gas and solid/liquid interface, Langmuir 8 (1992) 1961-1967.
[40] J.D. Le Grange, J.L. Markham, and C.R. Kurkjian, Effects of surface hydration on the deposition of silane monolayers on silica, Langmuir 9 (1993) 1749-1753.
[41] M.E. McGovern, K.M.R. Kallury, and M. Thompson, Role of solvent on the silanization of glass with octadecyltrichlorosilane, Langmuir 10 (1994) 3607-3614.
[42] J.B. Brzoska, I.B. Azouz, and F. Rondelez, Silanization of solid substrates: A step toward reproducibility, Langmuir 10 (1994) 4367-4373.
[43] A.N. Parikh, D.L. Allara, I.B. Azouz, and F. Rondelez, An intrinsic relationship between molecular structure in self-assembled n-alkylsiloxane monolayers and deposition temperature, J. Phys. Chem. 98 (1994) 7577-7590.
[44] W.R. Thompson and J.E. Pemberton, Characterization of Octadecylsilane and Stearic Acid Layers on Al_2O_3 Surfaces by Raman Spectroscopy, Langmuir 11 (1995) 1720-1725.
[45] R.R. Rye, G.C. Nelson, and M.T. Dugger, Mechanistic aspects of alkylchlorosilane coupling reactions, Langmuir 13 (1997) 2965-2972.
[46] M.J. Stevens, Thoughts on the Structure of Alkylsilane Monolayers, Langmuir 15 (1999) 2773-2778.
[47] R. Wang, J. Guo, G. Baran, and S.L. Wunder, Characterization of the state of order of octadecylsilane chains on fumed silica, Langmuir 16 (2000) 568-576.

[48] R. Wang and S.L. Wunder, Effects of silanol density, distribution and hydration state of fumed silica on the formation of self-assembled monolayer of n-octadecyltrichlorosilane, Langmuir 16 (2000) 5008-5016.
[49] H. Brunner, T. Vallant, U. Mayer, H. Hoffmann, B. Basnar, M. Vallant, and G. Friedbacher, Substrate effects on the formation of alkylsiloxane monolayers, Langmuir 15 (1999) 1899-1901.
[50] D. Cossement, Y. Delrue, Z. Mekhalif, J. Delhalle, and L. Hevesi, Self-assembled monolayers of branched alkylsilanes on polycrystalline titanium surfaces, Surface and Interface Analysis 30 (2000) 56-60.
[51] G. Philippin, J. Delhalle, and Z. Mekhalif, Comparative study of the monolayers of CH3-(CH2)n-SiCl3 and CH3-(CH2)(n)-PO(OH)(2), n=4 and 13, adsorbed on polycrystalline titanium substrates, Applied Surface Science 212 (2003) 530-536.
[52] M.P. Allen and D.J. Tildesley, *Computer Simulation of Liquids*. 1987, Oxford: Clarendon Press.
[53] D. Frenkel and B. Smit, *Understanding Molecular Simulation: From Algorithms to Applications*. 2nd ed. 2002, San Diego, CA: Academic Press.
[54] S.J. Klatte and T.L. Beck, Molecular Dynamics of Tethered Alkanes: Temperature-Dependent Behavior in a High-Density Chromatographic System, J. Phys. Chem. 97 (1993) 5727-5734.
[55] S.J. Klatte and T.L. Beck, Molecular Dynamics Simulations of Tethered Alkane Chromatographic Stationary Phases, J. Phys. Chem. 99 (1995) 16024-16032.
[56] S.J. Klatte and T.L. Beck, Microscopic Simulation of Solute Transfer in Reversed Phase Liquid Chromatography, J. Phys. Chem. 100 (1996) 5931-5934.
[57] I. Yarovsky, M.I. Aguilar, and M.T.W. Hearn, High performance liquid chromatography of amino acids, peptides, and proteins. CXXV. Molecular dynamics simulation of n-butyl chains chemically bonded to silica-based reversed-phase high-performance liquid chromatography sorbents, J. Chromatogr. A 660 (1994) 75-84.
[58] I. Yarovsky, M.I. Aguilar, and M.T.W. Hearn, Influence of the Chain Length and Surface Density on the Conformation and Mobility of n-Alkyl Ligands Chemically Immobilized onto a Silica Surface, Anal. Chem. 67 (1995) 2145-2153.
[59] I. Yarovsky, M.T.W. Hearn, and M.I. Aguilar, Molecular simulation of peptide interactions with an RP-HPLC sorbent, J. Phys. Chem. B 101 (1997) 10962-10970.
[60] J.T. Slusher and R.D. Mountain, A Molecular Dynamics Study of a Reversed-Phase Liquid Chromatography Model, J. Phys. Chem. B 103 (1999) 1354-1362.
[61] G.R. Gallaher and P.K.T. Liu, Characterization of ceramic membrane I. Thermal and hydrothermal stabilities of commercial 40 Å membranes, J. Membr. Sci. 92 (1994) 29-44.
[62] C.L. Lin, D.L. Flowers, and P.K.T. Liu, Characterization of ceramic membranes II. Modified commercial membranes with pore size under 40 Å, J. Membr. Sci. 92 (1994) 45-58.
[63] USFilter, *private communication*. 2000.
[64] M.M. Chehimi, M.L. Abel, J.F. Watts, and R.P. Digby, Surface chemical and thermodynamic properties of gamma-glycidoxy-propyltrimethoxysilane-treated

alumina: an XPS and IGC study, Journal of Materials Chemistry 11 (2001) 533-543.
[65] J.R. Miller, *Transport Properties of Native and Chemically Modified Gamma-Alumina Membranes*, in *Department of Chemical Engineering*. 1992, University of Texas at Austin: Austin, TX.
[66] Y.S. Lin and A.J. Burggraaf, Experimental studies on pore size change of porous ceramic membranes after modification, J. Membrane Sci. 79 (1993) 65-82.
[67] M. Trocha and W.J. Koros, A diffusion-controlled procedure to close pores in ceramic membranes, J. Membrane Sci. 95 (1994) 259-276.
[68] W.A. Steele, *The Interaction of Gases with Solid Surfaces*. 1974, Oxford: Pergamon.
[69] D.N. Theodorou and U.W. Suter, Detailed Molecular Structure of a Vinyl Polymer Glass, Macromolecules 18 (1985) 1467-1478.
[70] R.H. Boyd and P.V.K. Pant, Molecular Packing and Diffusion in Polyisobutylene, Macromolecules 24 (1991) 6325.
[71] P.V.K. Pant and R.H. Boyd, Molecular Dynamics Simulation of Diffusion of Small Penetrants in Polymers, Macromolecules 26 (1993) 679.
[72] N.F.A. van der Vegt, W.J. Briels, M. Wessling, and H. Strathmann, Free energy calculations of small molecules in dense amorphous polymers. Effect of the initial guess configuration in molecular dynamics studies, J. Chem. Phys. 105 (1996) 8849-8857.
[73] F. Muller-Plathe, Permeation of polymers - A computational approach, Acta Polymer 45 (1994) 259-293.
[74] B. Widom, Some topics in the theory of fluids, J. Chem. Phys. 39 (1963) 2808-2812.
[75] J.M.D. MacElroy, S.P. Friedman, and N.A. Seaton, On the origin of transport resistances within carbon molecular sieves, Chem. Eng. Sci. 54 (1999) 1015-1027.
[76] P.S. Rallabandi and D.M. Ford, Entropic and Energetic Selectivity in Air Separation with Microporous Materials, AIChE Journal 46 (2000) 99-109.
[77] G.R. Gallaher and P.K.T. Liu, Characterization of ceramic membranes. I. Thermal and hydrothermal stabilities of commercial 40 Å membranes, J. Membrane Sci. 92 (1994) 29-44.

DISTRIBUTION:

1 Turkan Aydogmus
Department of Chemical Engineering
Texas A&M University
College Station, TX 77843-3122

1 Asad Javaid
Department of Chemical Engineering
Texas A&M University
College Station, TX 77843-3122

1 David M. Ford
Department of Chemical Engineering
Texas A&M University
College Station, TX 77843-3122

1 MS0316 Aidan Thompson, 09235
1 MS0316 John Aidun, 09235
1 MS1411 Mark Stevens, 01834

1 MS0619 Central Technical Files, 8945-1
2 MS0899 Technical Library, 9616
1 MS0612 Review and Approval Desk, 9612
1 MS0323 LDRD Office, 01011